Available online at www.sciencedirect.com
SCIENCE DIRECT®
Advances in Space Research 36 (2005) 2497–2505
ADVANCES IN SPACE RESEARCH (a COSPAR publication)
www.elsevier.com/locate/asr

High accuracy satellite drag model (HASDM)

Mark F. Storz [a,*], Bruce R. Bowman [a], Major James I. Branson [b], Stephen J. Casali [c], W. Kent Tobiska [d]

[a] Air Force Space Command, Space Analysis Division, Peterson AFB, CO 80914, USA
[b] Air Force Space Battlelab, Schriever AFB, CO 80912, USA
[c] Omitron Inc., Colorado Springs, CO 80906, USA
[d] Space Environment Technologies, Inc., Pacific Palisades, CA 90272, USA

Received 19 October 2002; received in revised form 24 February 2004; accepted 25 February 2004

Abstract

The dominant error source in force models used to predict low-perigee satellite trajectories is atmospheric drag. Errors in operational thermospheric density models cause significant errors in predicted satellite positions, since these models do not account for dynamic changes in atmospheric drag for orbit predictions. The Air Force Space Battlelab's High Accuracy Satellite Drag Model (HASDM) estimates and predicts (out three days) a dynamically varying global density field. HASDM includes the Dynamic Calibration Atmosphere (DCA) algorithm that solves for the phases and amplitudes of the diurnal and semidiurnal variations of thermospheric density near real-time from the observed drag effects on a set of Low Earth Orbit (LEO) calibration satellites. The density correction is expressed as a function of latitude, local solar time and altitude. In HASDM, a time series prediction filter relates the extreme ultraviolet (EUV) energy index $E_{10.7}$ and the geomagnetic storm index a_p, to the DCA density correction parameters. The $E_{10.7}$ index is generated by the SOLAR2000 model, the first full spectrum model of solar irradiance. The estimated and predicted density fields will be used operationally to significantly improve the accuracy of predicted trajectories for all low-perigee satellites.
© 2005 COSPAR. Published by Elsevier Ltd. All rights reserved.

Keywords: Space weather; Satellite drag; HASDM; Atmospheric drag

1. Introduction

The High Accuracy Satellite Drag Model was an 18-month effort completed by the Air Force Space Battlelab in August 2002. Its goal was to improve Air Force Space Command's ability to meet stringent Space Surveillance Capstone Requirements for satellite trajectory prediction accuracy. For low-perigee satellites (<600 km altitude), these requirements are not consistently met, largely because current atmospheric density models have errors of 15–20% (Liu et al., 1983; Marcos, 1990). This can affect missions like maneuver planning, re-entry predictions, collision avoidance, and finding satellites with narrow field-of-view sensors. The Space Battlelab funded this initiative because of the substantial payback expected. It is also well suited to the Space Battlelab's project criteria of demonstrating unconventional ways of using existing data and technology to meet mission requirements, and being able to demonstrate this in 18 months or less. This initiative leveraged off an earlier Space Battlelab project (Marcos et al., 1998) that demonstrated the potential of the basic technique, even when only one satellite is used to extract the drag effects.

This initiative optimizes the earlier approach by simultaneously processing drag information from the trajectories of up to 75 inactive payloads and debris to solve for a dynamically changing global correction to the thermospheric and exospheric neutral density. The thermosphere is the layer of the atmosphere from 90 km to about 600 km altitude. The exosphere is the layer above the thermosphere. In this initiative, satellite

* Corresponding author. Tel.: +1 719 556 3715; fax: +1 719 556 3738.
E-mail address: mark.storz@peterson.af.mil (M.F. Storz).

0273-1177/$30 © 2005 COSPAR. Published by Elsevier Ltd. All rights reserved.
doi:10.1016/j.asr.2004.02.020

tracking observations (azimuth, elevation, range and range rate) from the Space Surveillance Network (SSN) were processed directly to derive the neutral atmospheric density. Thermospheric density correction parameters were computed along with the trajectory states of the calibration satellites in a single estimation process, known as the Dynamic Calibration Atmosphere (DCA). The density corrections reflect dynamic changes in the diurnal and semidiurnal variations (Hedin et al., 1980).

The initiative also capitalizes on the new SOLAR2000 model developed for the Space Environment Center by Space Environment Technologies, Inc. (Tobiska et al., 2000). This is the first-ever full solar spectrum model and acts like a data fusion engine, assimilating many different sources of solar irradiance data. It can generate various products related to the sun's electromagnetic radiation output. HASDM makes use of the extreme ultraviolet (EUV) wavelengths. This radiation is the major heat source in the thermosphere, causing the neutral density to change several orders of magnitude, throughout the 11-year solar cycle (Jursa, 1985). SOLAR2000 has recently been modified to produce a 3-day prediction of the EUV radiation in the form of an effective $F_{10.7}$ index based on the intensity of this radiation. This new index is known as $E_{10.7}$, and when input to existing models requiring $F_{10.7}$, is designed to boost their accuracy performance.

This project also included the development of a prediction model that maps the time series of solar and geomagnetic indices (including $E_{10.7}$) to the density correction parameters estimated by DCA. It also extrapolates information from the time series of the density correction coefficients using discrete Fourier and wavelet techniques. DCA's dynamic thermospheric density correction, together with the 3-day index prediction, significantly improves satellite trajectory estimation and prediction.

2. Background

The goal of this initiative is to estimate an accurate global correction to the modeled thermospheric neutral density deduced from drag effects on the trajectories of inactive satellites and orbiting debris, known as *calibration satellites*. The greater the thermospheric density, the faster low-perigee objects spiral inward. The US Air Force first explored the concept of estimating thermospheric density from satellite trajectories in 1995 at Air Force Space Command and Air Force Research Laboratory using Small Business Innovative Research funds. This led to the earlier Space Battlelab initiative, the Modified Atmospheric Density Model (MADM) (Marcos et al., 1998), which was completed in March 2000.

In MADM, the main parameter used to determine the density was the estimated ballistic coefficient. In the orbit determination process, this is a solve-for parameter, just like the elements of the satellite's state vector. The ballistic coefficient is a measure of how much the object is affected by atmospheric drag. The larger the ballistic coefficient, the greater effect the atmosphere has on the object (Liu, 1983). The true ballistic coefficient B_{true} and the true atmospheric density ρ_{true}, together with the speed V of the satellite, determine the drag acceleration a_{D} through the following approximate expression:

$$a_{\text{D}} = \frac{1}{2} B_{\text{true}} \rho_{\text{true}} V^2. \tag{1}$$

The true density ρ_{true} is generally not known, so the model density ρ_{model} is used instead. The estimated ballistic coefficient B_{model}, varies depending on the error in the modeled density ρ_{model}. If the model density is low when compared to the real density, then the estimated ballistic coefficient B_{model} is larger than its true value. Conversely, when the model atmospheric density is too high, B_{model} is smaller than its true value. Therefore, information about the bias in the atmospheric model is contained within the values for B_{model}. The "observed" drag acceleration a_{D} has nearly the same value, regardless of the value of ρ_{model} and B_{model}. Therefore,

$$a_{\text{D}} = \frac{1}{2} B_{\text{model}} \rho_{\text{model}} V^2. \tag{2}$$

This implies that, at every instant, $B_{\text{true}}\rho_{\text{true}} \cong B_{\text{model}}\rho_{\text{model}}$ and $\rho_{\text{true}} \cong (B_{\text{model}}/B_{\text{true}})\ \rho_{\text{model}}$. The ratio $B_{\text{model}}/B_{\text{true}}$ is referred to as the "scaled" estimated ballistic coefficient B_{scale}. Fig. 1 shows that Low Earth Orbit (LEO) satellites with different orbits generally exhibit similar trends in their B_{scale} time series (Snow and Liu, 1991). This indicates that B_{scale} can be used to correct the model density globally to obtain a rough estimate of the true density. Once a value for B_{true} is estimated by averaging successive values of B_{model} over a period of years (Bowman, 2002), then the value for ρ_{true} may be computed. MADM exploited this information from a single calibration satellite to deduce the bias of the model atmosphere, producing modest results. It reduced the root mean square (rms) of the epoch error by ~20% and reduced the error for a 1-day prediction by ~10% on average. HASDM reduces the rms of the epoch error by ~32% and reduces the error for a 1-day prediction by ~25% on average (Casali and Barker, 2002).

3. Dynamic calibration atmosphere

MADM employed a separate orbit determination process and a separate density estimation process. In

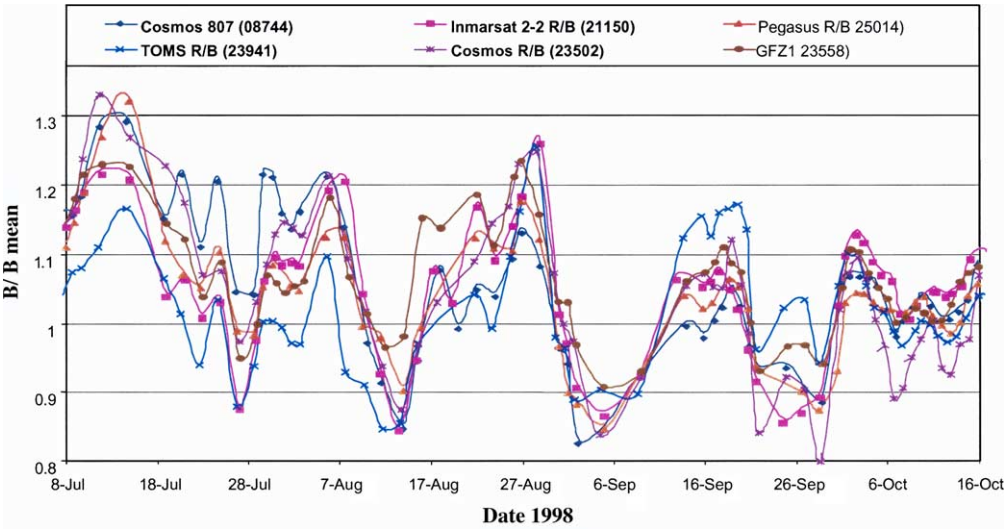

Fig. 1. Scaled ballistic coefficient histories ($B_{scale} = B_{model}/B_{true}$).

HASDM's Dynamic Calibration Atmosphere (DCA), these two processes are combined into a single estimation process. This is a weighted least squares differential correction across all calibration satellites that simultaneously solves for global density corrections and a state vector for each calibration satellite. DCA uses Space Surveillance Network (SSN) observations directly, thus avoiding any intermediate step of fitting the density correction to a time series of estimated ballistic coefficients B_{model} or energy dissipation rates (EDR). This approach also optimizes use of the detailed information contained in the original space surveillance observations. As in MADM, DCA uses the Jacchia, 1970 thermosphere as its base model (Jacchia, 1970). While MADM corrected only two global temperature parameters of the base model, DCA estimates 13 global density correction parameters. This global correction not only reduces the errors in the state error covariance for low-perigee satellites, but also makes these errors more realistic (less optimistic). In addition, the sensitivity of orbit accuracy to fit span length is significantly reduced. Once these density correction parameters are computed, they are output to a file so they can be accessed by users to improve orbit determination and prediction for all low-perigee satellites. DCA was developed by Omitron, Inc. in Colorado Springs, Colorado.

An important feature of DCA is its segmented solution approach. Although the state vector of each calibration satellite is estimated for a 1.5-day fit span interval, the density correction parameters are estimated on 3-h sub-intervals within the fit span. This approach is used to extract the time resolution needed to accurately determine the dynamically changing thermospheric density (Casali and Barker, 2002). This is especially important during geomagnetic storms, when the Joule heating of the auroral ovals drives rapidly changing density features. The observability of the parameters estimated for each segment is sufficient because of the large number (~75) of calibration satellites used, and because space surveillance tasking was increased to include every pass of each satellite over the sensors with 10 observations each.

In addition to estimating a density correction, the plan is to also employ a Segmented Solution for Ballistic coefficient (SSB). This is a technique whereby the estimated ballistic coefficient (B) is allowed to vary over the fit span. Fit spans of several days are divided into 1/2 to 3-h segments for which a separate ballistic coefficient is estimated. The plan is to apply the SSB technique after the DCA density corrections are applied, thus further improving the accuracy of the state vector estimate for the satellite trajectory. This technique may only be applied if there is sufficient tracking data to provide the observability needed for the segmented B estimates.

4. Temperature and density profiles

For this initiative, up to 75 calibration satellites were used simultaneously to solve for a global density correction field. This field corrects two local parameters in the vertical temperature profile leading to a unique density profile: a low-altitude parameter and a high-altitude parameter. DCA estimates a new set of parameters every 3 h. The number of coefficients is given by $(N_{low} + 1)^2 + (N_{high} + 1)^2$, where N_{low} and N_{high} are the degree of spherical harmonic truncation for the low- and high-altitude parameters respectively. The truncation degrees used in this effort are $N_{low} = 1$ and $N_{high} = 2$, for a total of 13 coefficients.

The low-altitude parameter is the so-called "inflection point temperature" T_x at 125 km altitude. The high-altitude parameter, the exospheric temperature T_∞, is the

asymptotic temperature the profile approaches with increasing altitude in the exosphere (>600 km altitude). The local temperature profile $T(z)$ as a function of altitude z is uniquely determined by T_x and T_∞. The local temperature profile leads to the local density profile through interpolation of density tables, which were produced by integrating the hydrostatic equation (from 90 to 105 km altitude) and the diffusion equation (above 105 km) (Hedin, 1991). The local values for T_x and T_∞ are both corrected indirectly through a *global* parameter known as the "nighttime minimum exospheric temperature" T_c. This is the principal parameter used in the standard Jacchia, 1970 model to describe the state of the entire thermosphere in response to solar extreme ultraviolet heating, and is given by the following expression:

$$T_c = 383 + 3.32F_{10.7} + 1.8(F_{10.7} - \bar{F}_{10.7}). \quad (3)$$

For the HASDM project, we replaced the $F_{10.7}$ index with the new $E_{10.7}$ index, which is based on the true extreme ultraviolet (EUV) heating of the thermosphere. B.R. Bowman developed the following empirical formula for T_c as a function of $E_{10.7}$ and $\bar{E}_{10.7}$:

$$T_c = 214 + 1.88E_{10.7} + 4.23\bar{E}_{10.7} - 0.01\bar{E}^2_{10.7} \quad (4)$$

In the modified Jacchia, 1970 model developed by the AFSPC Space Analysis Division (Storz, 1999), a ΔT_c correction is added to the standard T_c value to produce the corrected value

$$T'_c = T_c + \Delta T_c \quad (5)$$

The local exospheric temperature T'_∞ is obtained from T'_c in the same way the standard Jacchia, 1970 model obtains T_∞ from T_c; through multiplying by the diurnal variation factor $D(\delta, \phi, \lambda)$ (a function of solar declination δ, latitude ϕ and local solar time λ), and adding the contribution to T_∞ due to geomagnetic activity ΔT_G and the semiannual variation ΔT_S. The associated equation is as follows:

$$T'_\infty = T'_c D(\delta, \phi, \lambda) + \Delta T_G(a_p) + \Delta T_S(t, \bar{E}_{10.7}) \quad (6)$$

The local value for T'_x is then computed from the local exospheric temperature T'_∞ using the standard Jacchia, 1970 expression:

$$T'_x = 444.3807 + 0.02385T'_\infty - 392.8292 \times \exp(-0.0021357T'_\infty) \quad (7)$$

However, in the modified Jacchia model, the local inflection point temperature T'_x is further corrected by adding a ΔT_x correction to T'_x

$$T''_x = T'_x + \Delta T_x \quad (8)$$

The double prime indicates that this inflection point temperature is corrected twice; once through ΔT_c and again through ΔT_x. Both ΔT_c and ΔT_x are expressed in terms of independent spherical harmonic expansions in latitude and local solar time. Since local solar time is equivalent to the right ascension relative to the anti-solar point, it is actually an angular coordinate, not a time.

When $\Delta T_x = 0$, the temperature profile is identical to a standard Jacchia, 1970 profile for a given local exospheric temperature. Fig. 2 shows seven temperature profiles, each corresponding to a different local exospheric temperature T'_∞. These exospheric temperatures vary from 500 to 2000 K, representing the natural range of values. All temperature profiles start from a constant temperature of 183 K at 90 km altitude, the lower boundary. The temperature increases with altitude, exhibiting an inflection point at a fixed altitude of 125 km, indicated in Fig. 2 by the solid black vertical line. The temperature continues to increase and becomes asymptotic to the local exospheric temperature T'_∞. Fig. 3 shows seven temperature profiles, each corresponding to a different T''_x. The inflection point temperatures shown here range from 200 to 800 K. These T''_x values occur along the solid black vertical line at an altitude of 125 km. To explore the effect of changing T''_x only, the exospheric temperature in Fig. 3 was held constant at $T'_\infty = 2000$ K. The middle curve is nearly identical to the standard Jacchia, 1970 temperature profile with $\Delta T_x = 0$. Changing T''_x acts to flatten ($\Delta T_x \leqslant 0$) or steepen $\Delta T_x \geqslant 0$ the temperature gradient with altitude.

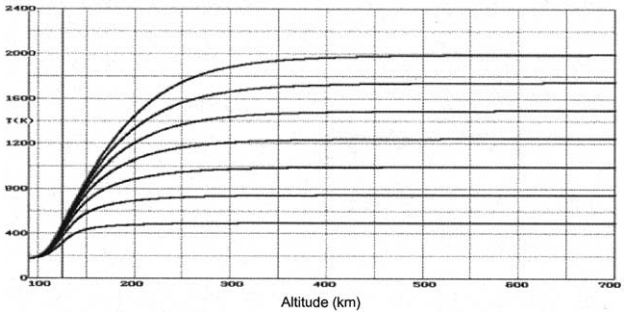

Fig. 2. Temperature profiles (T'_∞=500, 750, 1000, 1250, 1500, 1750, 2000 K with $\Delta T_x = 0$).

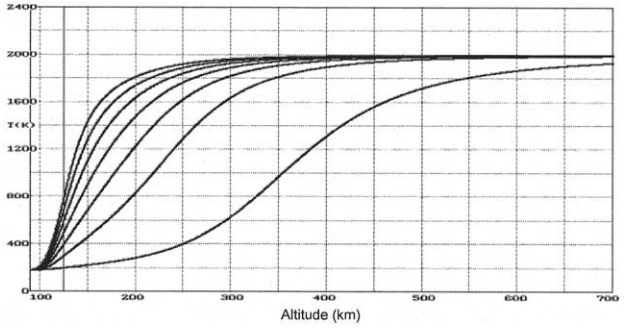

Fig. 3. Temperature profiles (T''_x = 200, 300, 400, 500, 600, 700, 800 K with T'_∞ = 2000 K).

For ΔT_x values less than approximately -100 K, a second inflection point appears at altitudes above 125 km. However, values for ΔT_x have magnitudes much smaller than ± 100 K, so this second inflection point never occurs in nature.

The local density profile is computed from the local temperature profile by integrating the hydrostatic and diffusion equations subject to the lower boundary conditions at 90 km altitude. Fig. 4 displays neutral density as a function of altitude and T'_∞. Fig. 5 displays neutral density as a function of altitude and T''_x. The key to understanding the relationship between the density profiles and the temperature profiles is to recognize that the thickness of a particular density interval (color band) measured along a horizontal (constant temperature) line, is proportional to the scale height (Jursa, 1985). Although the scale height is dependent on several things (temperature, mean molecular weight, diffusion coefficient and gravity acceleration), it is strongly proportional to the local temperature at a given altitude. Therefore, to a first approximation, the vertical density gradient is inversely proportional to the local temperature. The horizontal solid white line in Fig. 5 indicates the standard value ($T'_\infty = 487$ K) when $\Delta T_x = 0$ for an exospheric temperature of $T'_\infty = 2000$ K. Above ~250 km altitude, changing T''_x has an effect similar to multiplying the model density by a constant factor, or equivalently, shifting $\log_{10}(\rho)$ by a constant without significantly affecting the scale height, thus behaving like a thermospheric density 'constant bias term'. On the other hand, changing T_∞ alters the scale height as well as the density at all altitudes, thus behaving like a thermospheric density 'slope term'. Both terms are necessary to produce an accurate fit to the true density profile.

5. Density prediction technique

We make use of the 3-day prediction of the geomagnetic index a_p as well as a 3-day prediction of $E_{10.7}$, produced by the SOLAR2000 solar irradiance model. This model was developed by Space Environment Technologies Inc. for the Space Environment Center and other agencies (Tobiska et al., 2000). SOLAR2000 is the first-ever empirical full solar spectrum model. Its spectral resolution is 1 nm and extends from X-rays through

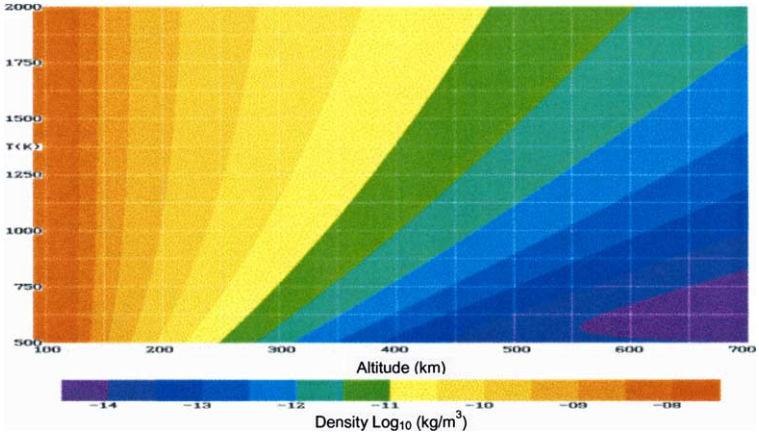

Fig. 4. Density versus altitude and exospheric temperature T'_∞ (with $\Delta T_x = 0$).

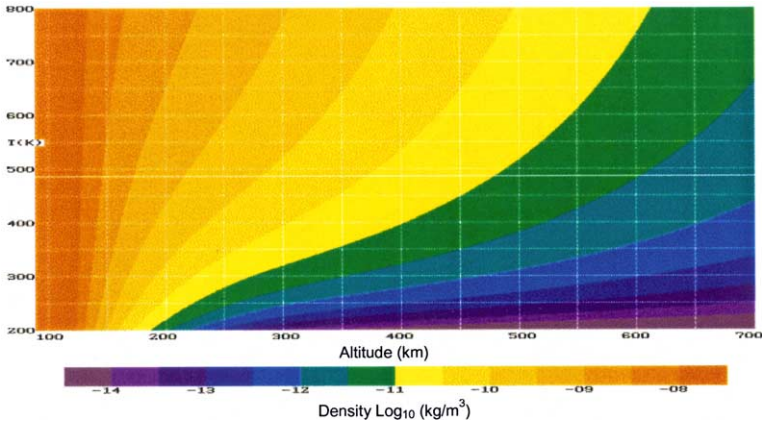

Fig. 5. Density versus altitude and inflection temperature T''_x (with $T'_\infty = 2000$ K).

the infrared (IR) spectrum. The temporal resolution extends from minutes to a full solar cycle (~11 years). It acts like a data fusion engine designed to ingest data from ultraviolet (UV) and extreme ultraviolet (EUV) sensors, ground-based optical sensors and total irradiance sensors and imagers. $E_{10.7}$ is based on the total solar irradiance integrated over EUV wavelengths affecting thermospheric heating and is averaged over the past 24 h. The resulting EUV flux was plotted versus the simultaneous $F_{10.7}$ indices and a curve was fit to the points. This curve is used to translate the integrated EUV flux to the $E_{10.7}$ index. A similar procedure was used to generate an $\bar{E}_{10.7}$ corresponding to the 81-day centered mean $\bar{F}_{10.7}$. When $E_{10.7}$ and $\bar{E}_{10.7}$ are used instead of $F_{10.7}$ and $\bar{F}_{10.7}$, they act to increase the accuracy of the thermospheric density model, even if that model was constructed using the $F_{10.7}$ indices. Currently, SOLAR2000 produces a now-cast and 3-day prediction of the $E_{10.7}$ and $\bar{E}_{10.7}$ indices.

The density correction coefficients from the Dynamic Calibration Atmosphere (DCA) are predicted out 3 days into the future using a prediction filter that relates these coefficients to the time series for $E_{10.7}$, $\bar{E}_{10.7}$ and a_p, as well as an extrapolation of the past time series of the coefficients themselves (Tobiska, 2002). All of the DCA coefficients are expressed as a separate function of the time series of their past values, as well as the predicted indices ($E_{10.7}$, $\bar{E}_{10.7}$ and a_p). This density prediction filter extrapolates the recent (last ~27 days) behavior of the time series of the DCA density correction coefficients. The behavior is deduced through discrete Fourier analysis of the frequency, phase, and amplitude of the coefficients as well as discrete wavelet analysis for short-term prediction of the transient part of the signal. The behavior of the coefficient time series is tied to the solar/geomagnetic heating indices. Therefore, the extrapolated time series is adjusted according to the values of the predicted indices. In this way, we can leverage off existing space forecast expertise in predicting the indices. This prediction filter significantly boosts the prediction accuracy of the HASDM thermospheric density model.

6. Satellite trajectory improvement

The primary objective of this effort is to improve the satellite trajectory accuracy at epoch and throughout the 3-day prediction. A related measure of success is enhanced realism of the satellite state error covariance over the same interval. A third criterion is the reduction in density error as reflected by reduced variation in the estimated ballistic coefficient (B). Assuming the true ballistic coefficient is roughly constant, reduced variation in estimated B indicates how well atmospheric density was corrected. All three metrics generally improved significantly with HASDM over the test period (January 15 to July 15, 2001).

Figs. 6 and 7 show the standard deviation (std) of the estimated ballistic coefficient (B) expressed as a percentage $[\mathrm{std}(B)/\bar{B}] \times 100\%$, where $\bar{B}$ is the mean of the estimated B over the 180-day HASDM test period. The highest percentages in these bar charts represent current operations. The middle percentages represent the fluctuations in estimated B after the DCA density corrections are applied. At epoch, using $E_{10.7}$ does not lower the B fluctuations relative to $F_{10.7}$. The lowest percentages (Solution Sigma) represent the error in estimating B due to observation errors. Fig. 6 shows the values for 60 of the calibration satellites, while Fig. 7 shows the values for 40 evaluation satellites, a set of satellites not used as calibration satellites by DCA. For Fig. 6, the percentage reduction in estimated B variation is $[\Delta\mathrm{std}(B)/\mathrm{std}(B)] \times 100\% = 74\%$, where Δ represents the operational std minus the std after applying the DCA density corrections. For Fig. 7, the percentage reduction is 53%. When combined, these percentages indicate an average reduction of about 65% as (see Table 1).

Figs. 8 and 9 show the root mean square (rms) of the vector magnitude (VMAG) error. VMAG is the distance of the predicted satellite position from its reference orbit position. The numerical scale for VMAG was removed for public release, but the figures show the relative decrease in VMAG when DCA density corrections are applied.

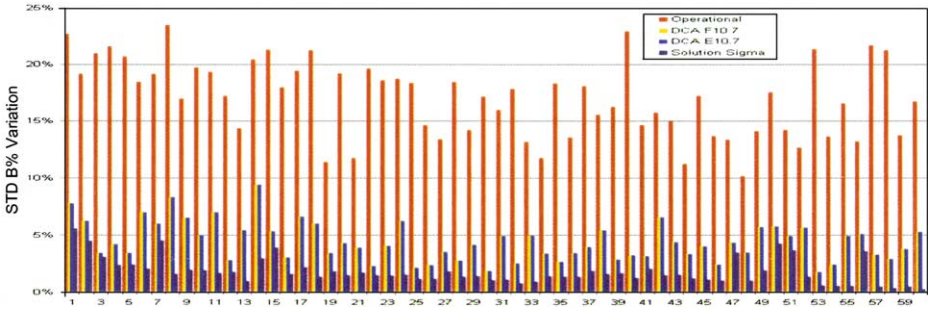

Fig. 6. Estimated ballistic coefficient (B) variability for 60 calibration satellites.

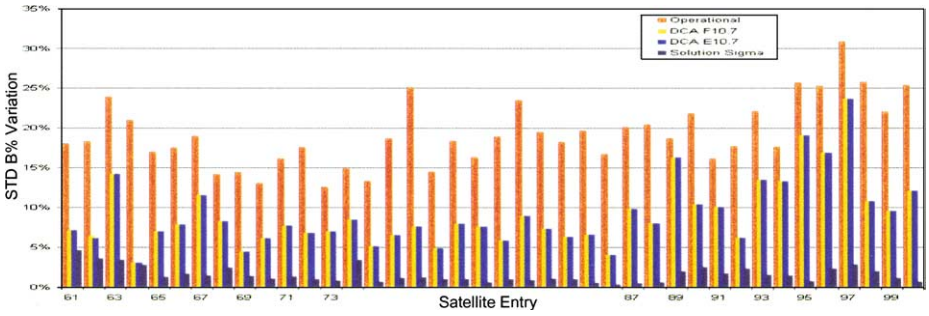

Fig. 7. Estimated ballistic coefficient (B) variability for 40 evaluation satellites.

Table 1
Percentage reduction in errors due to HASDM

Error type	Formula	Epoch	6 h	18 h	36 h	72 h
Position accuracy	$\frac{\Delta\text{rms(VMAG)}}{\text{rms(VMAG)}} \times 100\%$	32%	43%	30%	8%	12%
Covariance realism	$\frac{\Delta\text{rms}(\delta S/\sigma_S)}{\text{rms}(\delta S/\sigma_S)} \times 100\%$	46%	77%	31%	14%	7%
B Consistency	$\frac{\Delta\text{std}(B)}{\text{std}(B)} \times 100\%$	65%				

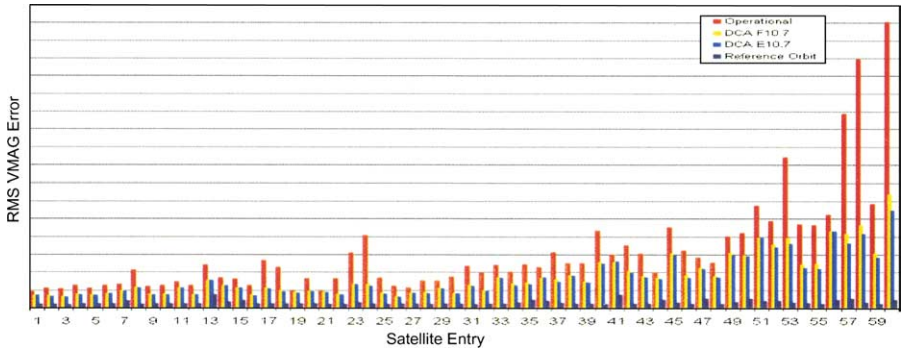

Fig. 8. Six-hour prediction error (VMAG) for 60 calibration satellites.

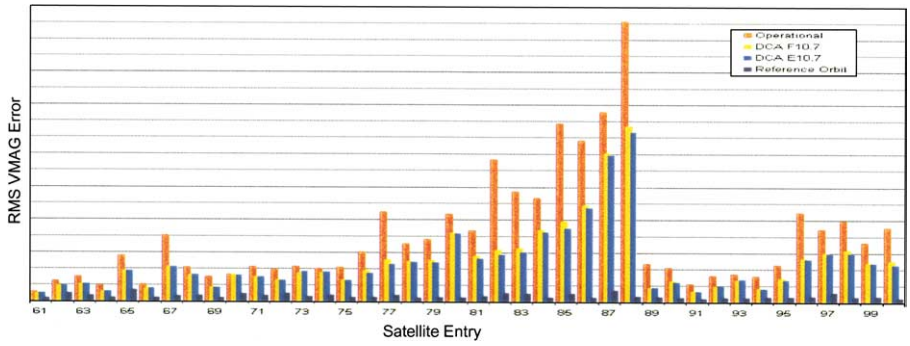

Fig. 9. Six-hour prediction error (VMAG) for 40 evaluation satellites.

The highest values represent current operations. The middle values represent the values after DCA is applied. Note that, for prediction, use of $E_{10.7}$ typically reduces the VMAG slightly when compared to use of $F_{10.7}$. The lowest values represent the VMAG error from the reference orbit error covariance matrix based on observational error. Fig. 8 shows the values for 60 of the calibration satellites, while Fig. 9 shows the values for 40 evaluation satellites.

For Fig. 8, the percentage reduction in VMAG error is given by $[\Delta\text{rms(VMAG)/rms(VMAG)}] \times 100\% = 46\%$ where Δ represents the operational rms minus the rms when the DCA density correction is applied using $E_{10.7}$. For Fig. 9, the percentage reduction is 40%. When

combined, these percentages indicate an average reduction of about 43% (see Table 1).

For current operations, the ratio of the empirical in-track error δS to the theoretical in-track error σ_S (based on observation error) is typically significantly greater than 1. If the theoretical error covariance were modeled perfectly, this ratio would be exactly 1. Although no figures were provided, the percentage reduction in the ratio $[\Delta\mathrm{rms}(\delta S/\sigma_S)/\mathrm{rms}(\delta S/\sigma_S)] \times 100\%$ indicates the improvement in covariance realism due to DCA density corrections as shown in Table 1. Again, Δ represents the operational rms minus the rms when the DCA correction is applied using $E_{10.7}$

DCA provides significant improvement over current operations for prediction times of 0–18 h, and exhibits diminishing returns after 36 h. DCA does not reduce epoch accuracy to the level achieved using the Segmented Solution for Ballistic coefficient (SSB) reference orbits, despite showing a substantial improvement in comparison to the operational accuracy (lying about halfway between the two). Therefore, to maximize operational benefit, it will probably be necessary to use SSB in conjunction with DCA for moderate to high-energy dissipation rate (EDR) satellites to reduce satellite-specific errors.

7. Conclusion

Atmospheric density models for computing drag forces on satellites are a major source of inaccuracy in trajectory predictions for low-perigee satellites. This deficiency can result in serious errors in the predicted position of satellites, especially those with perigees below 600 km altitude, the layer known as the thermosphere. Many of these objects are of high interest to Space Control missions.

Current thermospheric density models do not adequately account for dynamic changes in atmospheric drag for orbit predictions, and no significant operational improvements have been made since 1970. Lack of progress is largely due to poor model inputs in the form of crude heating indices, as well as poor model resolution, both spatial and temporal. The High Accuracy Satellite Drag Model (HASDM) initiative uses the Dynamic Calibration Atmosphere (DCA) algorithm to solve for thermospheric neutral density near real-time from the observed drag effects on a set of low-perigee inactive payloads and debris, referred to as *calibration satellites*. Many different calibration satellites with different orbits may be exploited to recover a dynamically varying global density field. The greater the number of calibration satellites, the better the accuracy. For this initiative, we used up to 75 such satellites.

There are four major innovations within this initiative that contribute to improvement in the way satellite drag is determined and predicted:

- *Dynamic calibration atmosphere (DCA)*: This algorithm estimates a dynamic global density correction that models the true density to within a few percent. It estimates this density correction every 3 h.
- *EUV index* ($E_{0.7}$): This index is generated by the new SOLAR2000 model, the first full spectrum model of solar electromagnetic radiation. Not only does this index better represent the true heating of the thermosphere due to solar extreme ultraviolet (EUV) radiation, but also can be more accurately predicted out 3 days or more.
- *Prediction filter for DCA corrections*: This density prediction filter extrapolates the recent (last ~27 days) behavior of the time series of the DCA density correction coefficients. The behavior is deduced through wavelet analysis and Fourier analysis of the frequency, phase, and amplitude of the coefficients. The extrapolated time series is adjusted according to the values of the predicted solar and geomagnetic indices.
- *Segmented solution for ballistic coefficient (SSB)*: This is a technique whereby the estimated ballistic coefficient is allowed to vary over the fit span. Fit spans of several days are divided into 1/2 to 3-h segments for which a separate ballistic coefficient is estimated. For operations, the plan is to apply the SSB technique after the DCA density corrections are applied, thus further improving the accuracy of the satellite trajectory estimates.

A fair amount of success has come from previous efforts using spherically symmetric density corrections (Marcos et al., 1998; Nazerenko et al., 1998). However, HASDM's horizontally and temporally varying correction produces a significantly more accurate density solution. The estimated spherical harmonic coefficients may be readily used to specify and predict a corrected global density field which can be applied to special perturbations orbit determination and prediction for any low-perigee satellite. Accuracy requirements for all Space Control missions should be met at a much better rate. This initiative can also provide a useful neutral density database for basic research.

Acknowledgement

We thank our colleagues, Dr. Joseph J.F. Liu and Mr. Wilbert F. Craig, for their valuable contributions and insight. We also thank Mr. William N. Barker of

Omitron, Inc. and Mr. James G. Miller of Mitre Corp. for essential contributions to the HASDM effort. Finally, we thank Mr. Frank A. Marcos of Air Force Research Laboratory for his valuable suggestions and guidance.

References

Bowman, B.R. True satellite ballistic coefficient determination for HASDM, AIAA-2002-4887, in: AIAA/AAS Astrodynamics Specialist Conference Monterey, CA, August 2002.

Casali, S.J., Barker, W.N. Dynamic calibration atmosphere (DCA) for the high accuracy satellite drag model (HASDM), AIAA-2002-4888, in: AIAA/AAS Astrodynamics Specialist Conference, Monterey, CA, August 2002.

Hedin, A.E., Spencer, N.W., Mayr, H.G. The semidiurnal and terdiurnal tides in the equatorial thermosphere from AE-E measurements. J. Geophys. Res. 85, 1787–1791, 1980.

Hedin, A.E. Extension of the MSIS thermosphere model into the middle and lower atmosphere. J. Geophys. Res. 96, 1159–1172, 1991.

Jacchia, L.G. New static models of the thermosphere and exosphere with empirical temperature profiles, Smithsonian Astrophysical Observatory Special Report 313, May 1970.

Jursa, A.S. (Ed.). Handbook of Geophysics and the Space Environment. Air Force Geophysics Laboratory, (USAF), 1985.

Liu, J.J.F. Advances in orbit theory for an artificial satellite with drag. J. Astronautical Sci. XXXI (2), 165–188, 1983, Apr–Jun.

Liu, J.J.F., France, R.G., Wackernagel, H.B. An analysis of the use of empirical atmospheric density models in orbital mechanics, in: AAS/AIAA Astrodynamics Specialist Conference, Lake Placid, NY, August 1983.

Marcos, F.A. Accuracy of atmosphere drag models at low satellite altitudes. Adv. Space Res. 10 (3), 417–422, 1990.

Marcos, F.A., Kendra, M.J., Griffin, J.M., Bass, J.N., Liu, J.J.F., Larson, D.R. Precision low earth orbit determination using atmospheric density calibration. Adv. Astronautical Sci. 97 (1), 515–527, 1998, AAS.

Nazerenko, A.I., Cefola, P.J., Yurasov, V. Estimating atmospheric density variations to improve LEO orbit prediction accuracy, AAS-98-190, in: AAS/AIAA Space Flight Mechanics Meeting, Monterey, CA, February 1998.

Snow, D.E., Liu, J.J.F. Atmospheric variations observed from orbit determination, in: AAS/AIAA Astrodynamics Specialist Conference, Durango, CO, August 1991.

Storz, M.F. Satellite drag accuracy improvements estimated from orbital energy dissipation rates, in: AAS/AIAA Astrodynamics Specialist Conference, Girdwood, AK, August 1999.

Tobiska, W.K., Woods, T., Eparvier, F., Viereck, R., Floyd, L., Bouwer, D., Rottman, G., White, O.R. The SOLAR2000 empirical solar irradiance model and forecast tool. J. Atmos. Solar-Terr. Phys. (Apr), 2000.

Tobiska, W.K. $E_{10.7}$ use for global atmospheric density forecasting in 2001, AIAA-2002-4892, in: AIAA/AAS Astrodynamics Specialist Conference, Monterey CA, August 2002.